Spontaneous development of optical activity during freezing. A kinetic lattice model

J. G. Harris and F. H. Stillinger
AT&T Bell Laboratories, Murray Hill, New Jersey 07974

(Received 14 December 1989; accepted 20 February 1990)

Spontaneous optical resolution, a process by which a racemic mixture develops optical activity without the intervention of any external optically active reagent or field, has been observed during the freezing of certain organic compounds, i.e., 1,1′ binaphthyl. We develop a two-dimensional lattice model with simple triatomic molecules to investigate this phenomenon. Simulations verify that this model has a first-order phase transition from a racemic fluid phase to a chiral crystal. At high density and deep undercooling this phase transition proceeds by rapid nucleation of small clusters followed by a much slower flocculation of the clusters through the motion of grain boundaries. At low density homogeneous nucleation and growth by the addition of single particles or very small clusters is capable of producing crystals with close to the maximum possible optical activity from a racemic mixture. A requirement for spontaneous optical resolution is that the two optical isomers can interconvert within the time scale of the observed crystal growth. Even though the thermodynamic stability of the racemic liquid and the chiral solid are independent of the interconversion rate, when it is zero or extremely low the optical activity is fixed at its initial value and crystallization is inhibited.

I. INTRODUCTION

The molecular biology of terrestrial life reveals a strong bias in the population of optical isomers. This bias at first seems mystifying, since the initial composition of the early earth must have been racemic and only very weak chiral perturbations could have been present during the early chemical evolution of our biosphere. However there are circumstances in which a spontaneous chiral symmetry breaking can arise, and one or more of these might have played a role in the development of our asymmetric biochemistry. This paper investigates one of those scenarios.

This scenario is a spontaneous optical resolution which occurs during freezing. It has been identified in two types of systems. In the first, the achiral compounds crystallize into enantiomorphous crystals in one of the three chiral space groups.[1,2] Quartz is one of the most common examples. In the second, the subject of this paper, the optical isomers can interconvert or racemize on the time scale of the crystallization process.[2,3] They can form a crystal composed of predominantly one optical isomer, presuming it is kinetically accessible and is the thermodynamically stable form. When the racemic liquid is cooled below the freezing point, the fluctuations producing the initial critical nuclei determine the optical activity of the final product. If the system is cooled slowly enough, a crystal formed from one nucleus is likely to dominate the entire system, which will then exhibit strong optical activity.

Spontaneous optical resolution has been observed when racemization occurs through a bond breakage which disrupts the chiral center[2,4,5] or by a bond rotation around a high potential energy barrier.[2,6–12] The 1,1′ binaphthyl molecule is an excellent example of the latter case.[7–12] Because of steric hindrance the molecule's most stable conformation is twisted and lacks a center of inversion symmetry. The steric hindrance is weak enough for the molecule to occasionally rotate about the bond between the two naphthyl groups, so that when dissolved in benzene at room temperature, the half life of a conformation is about 10 h.[9] During crystallization, it is possible to produce from a racemic mixture a single crystal composed almost entirely of one of the two optical isomers. Both of the two chiral crystals are produced with the same probability.[7]

In a pure, ideal system, spontaneous optical resolution begins with homogeneous nucleation and continues through crystal growth. The modern theory of homogeneous nucleation is based on the classical model originally developed by Becker and Doring.[13,14] In the classical nucleation theory clusters of solid-like material develop spontaneously in the fluid. The nuclei grow and shrink by the addition or loss of individual particles from the liquid. Clusters smaller than a critical nucleus size usually dissolve and those larger grow to form macroscopic crystals. This critical nucleus represents the lowest activation barrier to freezing. The theory also assumes that after a time lag, the distribution of subcritical nuclei achieves a steady state and the concentration of n molecule nuclei is

$$C_n = C\exp\{-[(\Delta g)n + b\gamma n^{(d-1)/d}]/k_B T\}, \quad (1)$$

where Δg is the bulk free-energy difference per molecule between the solid and the liquid phases, γ is surface free energy between the phases, $bn^{(d-1)/d}$ is the average surface area of the n-molecule clusters, C is the pre-exponential factor which has a weak and usually neglected temperature dependence, T is the temperature, and k_B is the Boltzmann constant. In the nucleation of the solid, Δg is obtained from the thermodynamic properties of the solid and the supercooled liquid, but because independent measurements of γ are generally unavailable this latter quantity is determined from the variation of the nucleation rate with temperature (i.e., see Ref. 15 for such a determination from silicon).

 0021-9606/90/106140-12$03.00

We can directly observe the formation of the solid phase and test various assumptions of nucleation theory through computer simulations. So far only simple systems—argon and other spherical molecules,[16,17] rubidium,[18] and simple lattice gases[19–21]—have been studied using simulations. The molecular dynamics simulations of Swope and Andersen for argon show that in the early stages of solidification a steady-state distribution of 3–10 atom nuclei develops. Although this distribution is of the form of Eq. (1), the structure of the nuclei both above and below the critical size is inconsistent with the classical theory in that they consist of a mixture of fcc and hcp atom arrangements.[16] The argon in the simulation anneals to a pure fcc lattice after all of the atoms have been incorporated into nuclei.

Because the molecules involved in spontaneous optical resolution (i.e., the binaphthyl) are too complicated to study conveniently using molecular dynamics, we have developed a simple two-dimensional lattice model, which we call the chiral trimer model. The kinetics of our model are rapid enough to observe freezing on the time scale of a computer simulation. We are able to verify the existence of a freezing transition and the occurrence of spontaneous optical resolution in this model, as well as to test the applicability of homogeneous nucleation theory. Section II defines the chiral trimer model. Section III presents the techniques used in studying the dynamics and equilibrium properties of the model. Section IV discusses its equilibrium properties. Section V exhibits the results of "dynamical simulations" of the first-order phase transition.

II. THE MODEL

The chiral trimers reside on a two-dimensional square lattice and consist of three atoms, O, X, and C (Fig. 1), where C is the "central atom" to which O and X are both bonded on adjacent lattice sites. The bonds OC and XC are at right angles to each other so that a molecule cannot remain in the lattice plane and be superimposed upon its mirror image.

Three types of interactions determine the properties of this system. First, an exclusion interaction forbids the occupation of a lattice site by more than one atom. Second, atoms from different molecules experience an attractive "van der Waals" interaction ϵ_N when they are on nearest neighbor sites. Third, molecules whose central atoms are two lattice sites apart along a lattice direction and whose orientation and chirality are identical experience an attractive interaction, ϵ_C, which we call the "directional interaction." Thus for a system of nonoverlapping molecules the internal energy is

$$U = M_N\epsilon_N + M_C\epsilon_C, \tag{2}$$

where M_N and M_C are the numbers of van der Waals and directional interaction pairs occurring in the system.

The directional interaction provides the origin of possible spontaneous optical resolution. When $\epsilon_C > 2\epsilon_N$, the lowest energy structure becomes a compact crystal consisting of interdigitating lines of oriented molecules as shown in Fig. 2(a). These crystals are achiral and highly degenerate, since the interaction energy of adjacent lines of molecules is independent of their chiralities and orientations. When $\epsilon_C < 2\epsilon_N$ the lowest energy structure is a chiral crystal similar to that shown in Fig. 2(b). Because there are four orientations and two chiralities of the molecules and four sublattices on which to place all of the C atoms, this state has a 32-fold degeneracy. Under the latter condition which includes all cases studied in this work, the system can exhibit spontaneous optical resolution.

It is useful at this point to mention some of the types of excitations that can be observed in the crystalline phase—flips, interstitials, and vacancies. At a flip a molecule rotates or inverts and moves one lattice spacing to maximize the number of van der Waals interactions. The energy of the flip is $-4\epsilon_C + 2\epsilon_N$ [Fig. 3(a)]. A vacancy adds $-4\epsilon_C - 4\epsilon_N$ to the energy of the crystal [Fig. 3(b)]. The creation of an interstitial requires the disruption of the arrangement of some neighboring molecules and hence adds an energy of $-7\epsilon_C + 10\epsilon_N$ [Fig. 3(c)].

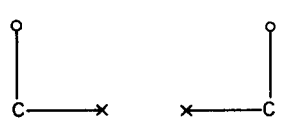

FIG. 1. Simple model triatomic molecule studied in this work.

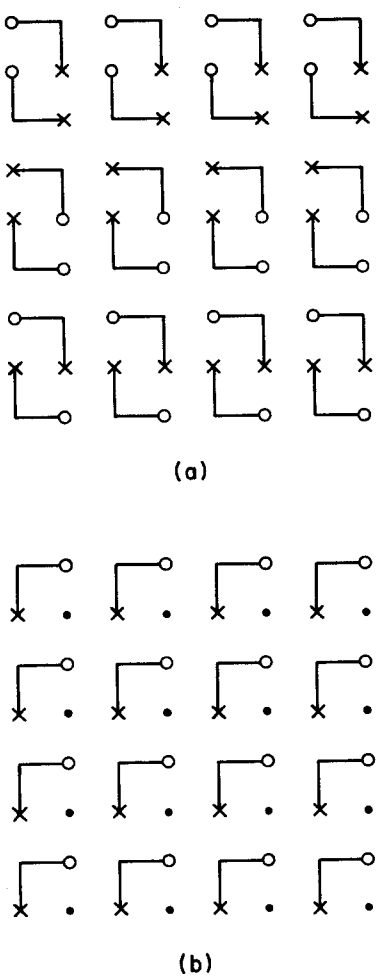

FIG. 2. Ground-state crystal when (a) $\epsilon_C > 2\epsilon_N$ and (b) $\epsilon_C < 2\epsilon_N$.

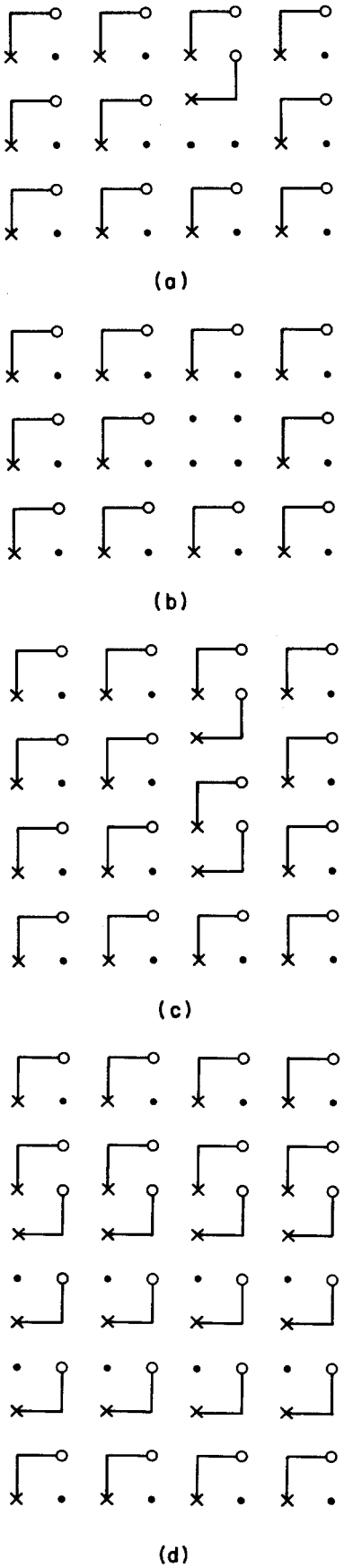

FIG. 3. Defects occurring in the chiral crystal: (a) a simple flip and rearrangement, (b) a vacancy, (c) an interstitial, and (d) the interdigitating low-energy (upper) and noninterdigitating high-energy (lower) grain boundaries.

The two complementary types of grain boundaries are shown in Fig. 3(d). In the first, bonds from molecules on the two grains interdigitate. In the second, at the grain boundary, the bonds in molecules of each crystal grain lie parallel to the boundary as shown by the lower grain boundary in Fig. 3(d). The interdigitating grain boundary lowers the energy of the crystal when $\epsilon_C > 3\epsilon_N$, but it must be paired with the other type of grain boundary (which is less favorable) except in the case of a single boundary in an isolated crystal. Unless the neighboring molecules are rearranged, none of the molecules at the interdigitating grain boundary can undergo any of the motions we allow in our simulations (discussed below). It is therefore effectively pinned during the simulation. Such a grain boundary can be destroyed when other more mobile types of grain boundaries or defects collide with it.

III. METHODS

The Monte Carlo simulations that we have used in determining equilibrium properties are carried out using a Metropolis sampling,[22] in which the basic moves are the translation of a molecule by one lattice spacing in one of the four lattice directions, the rotation of the molecule clockwise or counterclockwise by 90°, and the inversion of the molecule to its mirror image by the translation of the center unit across the diagonal between the O and X units. A molecule and one of the seven moves are selected from a random uniform distribution. The configuration resulting from the move is accepted with a probability of min $\{1, \exp[-(U_f - U_i)/k_B T]\}$, where U_i and U_f are the energies of the configurations before and after the move, respectively. If the configuration resulting from the move is not accepted, then the configuration prior to the move is reused as the next configuration in the series. The equilibrium statistics reported in this work were taken from 80×80 and 40×40 lattices with periodic boundary conditions.

In order to vary the inversion rate R_I in the dynamical simulations, we modify this algorithm slightly by adjusting the relative probabilities of selecting a translation, a rotation, or an inversion. Of course, the net transition probabilities (taking into account the acceptance probability) of the Monte Carlo steps must satisfy the detailed balance condition, e.g., the probabilities of selecting the two rotations must be equal. We studied two cases, one in which all seven moves are equally probable ($R_I = 1$) and another in which the inversion move is never chosen ($R_I = 0$). One unit of time τ is defined as one attempted move per molecule and the density is defined as the ratio of the number of molecules to the number of lattice sites ($\rho = 1/3$ is close packed). Temperature is defined by fixing ϵ_N at -1.0. Most of the computations were performed on a Cray XMP/24 at a rate of about a million attempted moves per cpu minute. The dynamical simulations reported in this work were performed with $\epsilon_C = -3.5$ at two densities, $\rho = 0.25$, the density of the perfect crystal, and $\rho = 0.125$, both using 80×80 lattices unless otherwise noted.

Among the properties tabulated are the directional interaction energy per molecule, the van der Waals interaction

per molecule, the cluster size distribution, and the rate of cluster growth, flocculation, and shrinkage. In this work two molecules are defined to be in the same cluster (or crystallite) if they interact through a directional interaction directly or with two other molecules which are both in the same cluster. To monitor cluster growth we define the "child" of a cluster appearing in a configuration as the cluster in some later configuration that has the largest number of the original cluster's molecules. In the event of a tie, the original cluster is considered to have shrunk, since it is broken up. A cluster has shrunk if its child is smaller than it is. A cluster has grown if its child is larger and no other cluster in the earlier configuration contributes as many or more molecules to the child. The cluster has flocculated onto another cluster if its child is larger, but some other cluster in the earlier configuration has contributed as many or more molecules to the child. Clearly these definitions neglect the fact that molecules in enclosed defects might be considered part of the crystallite; however, at temperatures below $T = 1.5$ such defects are rare in equilibrium crystals.

We occasionally use a chiral order parameter, the average chirality of all of the molecules. The chirality of the molecule is the component perpendicular to the lattice plane of the cross product of its two bonds and thus can be ± 1. The mean chiral order parameter is 0 in the fluid and ± 1 in the perfect crystal. At densities approaching the perfect crystal density, the chiral order parameter is a poor measure of the degree of crystallization because the contributions in different grains tend to cancel.

IV. EQUILIBRIUM PROPERTIES OF THE MODEL

We have studied the equilibrium properties of the chiral trimer model for the case $\epsilon_C = -3.5$ and $\epsilon_N = -1.0$ using both a primitive mean field theory and Monte Carlo simulations. The mean field (Bragg–Williams) theory gives a qualitative picture of the phase diagram, but is quantitatively very inaccurate. In the Bragg–Williams approximation the athermal insertion probability of a molecule is $(1-3\rho)^3$. Thus, in the mean field approximation the free energy is given by

$$f = k_B T\left[\sum_{i=1}^{8} \rho_i \ln \rho_i + 2\rho + (1-3\rho)\ln(1-3\rho)\right] + 12\epsilon_N\rho^2 + 2\epsilon_C \sum_{i=1}^{8} \rho_i^2, \quad (3)$$

where the ρ_i's are the densities of the molecules in each of the eight possible rotational-chiral states. The last two terms are the contributions from the van der Waals and the directional interactions, respectively. Equation (3) underestimates the free energy of the perfect crystal by a factor of 4 and thus at best can only give a rough qualitative picture of the phase diagram. The phase diagram is determined by methods similar to those applied in the mean field theory of the Potts model.[23] Because the mean field free energy is invariant to all permutations of the eight densities, it is parameterized by two variables, ρ, the total density, and s, the fraction of molecules in one of the eight states, which we take to be the first by convention. Thus $\rho_1 = s\rho$, and $\rho_i = (1-s)/8\rho$ when $i > 1$. At temperature T and density ρ, s is adjusted to minimize the free-energy function given by Eq. (3). Then, the double tangent construction is used to locate the coexistence points on the T-ρ phase diagram. The disorder characteristic of the liquid state requires that $s = 0.125$. Any other value implies orientational ordering and optical activity. Only one such phase, the solid, is observed in these calculations. There are seven other possible solid states differing only by the particular orientational-chiral species that are present in excess. A sketch of the phase diagram when $\epsilon_C = -3.5$ is shown in Fig. 4(a). As ϵ_C increases, the boundary between the liquid region and the crystal region will move to higher temperature, until the liquid–vapor transition disappears entirely and is replaced by just one fluid to crystal transition such as that in the mean field phase diagram for $\epsilon_C = -14$, shown in Fig. 4(b).

The Monte Carlo simulations at $\epsilon_C = -3.5$ indicate that as in Fig. 4(b), the model has only a fluid–solid transition. At $\rho = 0.25$, $\rho = 0.125$, and at $\rho = 0.0625$, the vapor condenses directly to the crystalline phase. Because of the slow convergence of simulations at high densities, we have

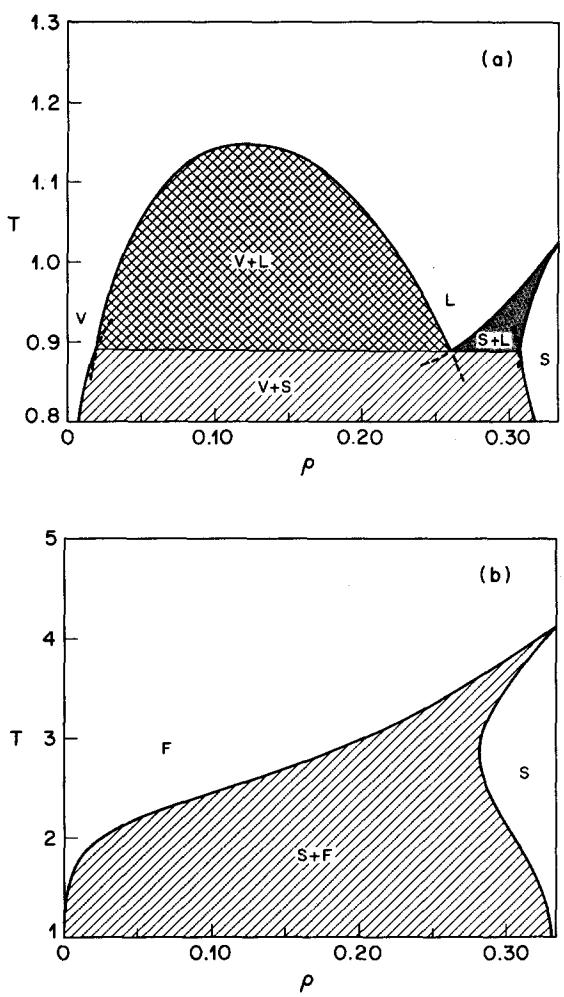

FIG. 4. Phase diagram of the chiral trimer model as predicted by mean field theory when (a) $\epsilon_C = -3.5$ and (b) $\epsilon_C = -14.0$. $\epsilon_N = -1.0$ in this work. The phases are vapor (V), liquid (L), solid (S), and fluid (F).

not used the Monte Carlo simulations to explore the high density region of the phase diagram, but the lack of a liquid–vapor transition at the temperatures and densities studied suggests that the real phase diagram of the chiral trimer model for $\epsilon_C = -3.5$ resembles the mean field phase diagram for the large values of ϵ_C shown in Fig. 4(b). We did not determine by Monte Carlo simulation whether the additional liquid–vapor phase transition occurs for some $\epsilon_C < 2.0\epsilon_N$, hence it is conceivable that an $|\epsilon_C|$ low enough to allow this transition would be too low for the chiral crystal to be stable.

The phase diagram obtained from the Monte Carlo simulations implies that significant improvements are needed beyond any mean field theory. The most significant improvement would be to eliminate the neglect of the correlations between the orientations of molecules in the crystal. This could be done by introducing an additional order parameter designating one of four sublattices a molecule's center could lie on. The four sublattices would be distinguished by whether their x and y coordinates are odd or even. It is also necessary to improve the treatment of the excluded volume. Unfortunately these improvements will destroy the invariance of f to permutations of the eight densities and will complicate the locating of the equilibrium phases.

In Fig. 5, we show the directional energy as a function of temperature at $\rho = 0.25$. The rapid change in the directional intermolecular energy at $T \approx 1.75$ indicates that the transition is first order with a latent heat of 3.4 ± 0.1.

A more precise estimate of the transition temperature can be made by computing the slope of the linear portion of the log C_n vs n curve at several temperatures just above the freezing point, and extrapolating the plot of slopes vs temperature to the point where the slope becomes zero. The logarithm of the crystallite distribution is plotted at four temperatures in Fig. 6. It can be seen that as the temperature decreases, the absolute value of the slope of the linear portion of the curve decreases. It should approach zero at the freezing point, because this slope is proportional to the free-energy difference between the liquid and the solid phase. Extrapolation to the point at which the slope vanishes predicts a transition temperature of $T = 1.73$. At $T = 1.725$, crystallite sizes of well over 100 molecules can be observed. The accuracy of this extrapolation is limited by the increasing relative importance of the surface term in Eq. (1) as the freezing temperature is approached.

We have also attempted to extrapolate the crystallite distributions to below the melting point to estimate the critical cluster sizes. Our data are insufficient to obtain all three parameters in Eq. (1) through a least-squares fit. However, Δg can be estimated using heat capacity data from both the crystal and liquid phases and the entropy of sublimation. This Δg can then be inserted into Eq. (1), and the two remaining parameters determined. The surface tension and the prefactor are assumed to be temperature independent over the modest temperature range employed and fits to data at 1.8, 1.85, and 1.9 predict $b\gamma = 1.7$. The critical nucleus size is $[b\gamma/(2\Delta g)]^2$ which is 208 molecules when $T = 1.7$, 13 when $T = 1.6$, 5 when $T = 1.5$, and 2 when $T = 1.3$. This suggests that homogeneous nucleation theory would break down for any $T \leqslant 1.6$.

Classical nucleation theory also assumes rather compact clusters which would be almost square in our model. By comparing the average number of directional interactions per molecule in all clusters of a given size with the minimum (all the molecules in one line) and maximum (a compact cluster) for a cluster of that size, we can measure the "compactness" of the cluster. In Fig. 7, we compare the average number of directional interactions in crystallites just above the melting point with the minimum and maximum possible values. The difference between the temperatures above the

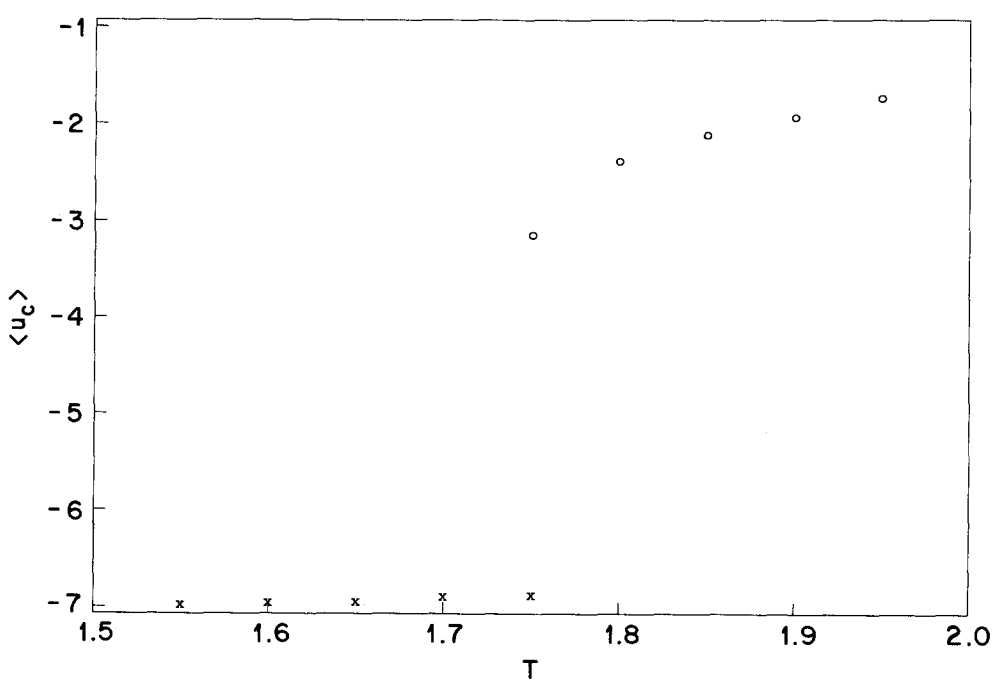

FIG. 5. Directional interaction energies per molecule, $\langle u_C \rangle$, at $\rho = 0.25$ for the liquid (O) and solid phases (X) as a function of temperature, computed from a 40×40 lattice with 400 molecules for the solid and for the liquid at $T = 1.95$, and from an 80×80 lattice with 1600 molecules for the other cases. At $T = 1.75$ the freezing/melting does not occur during the simulation.

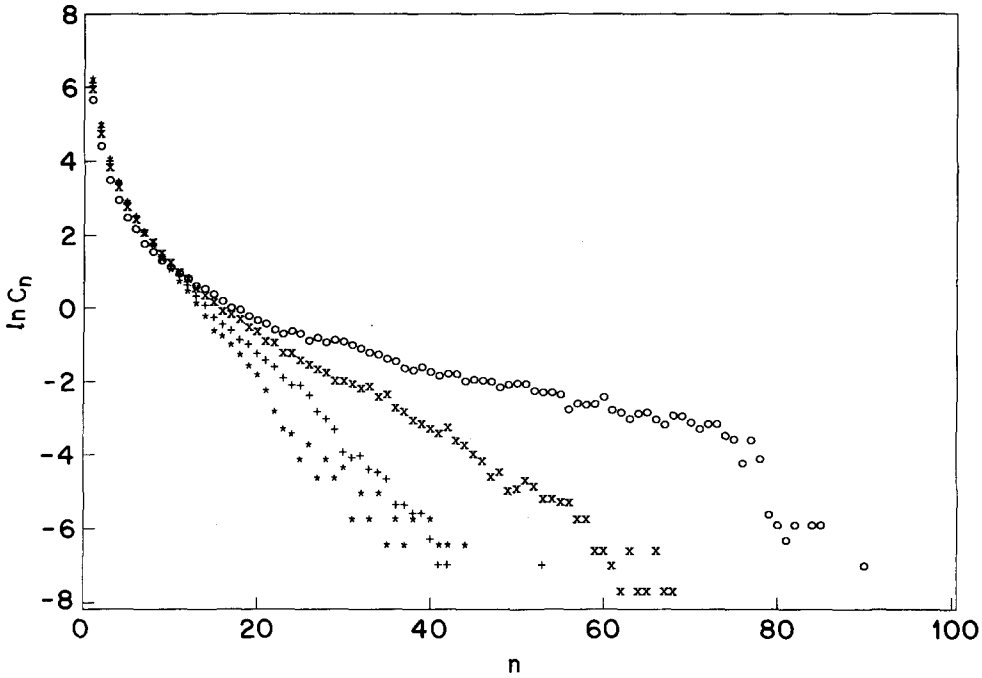

FIG. 6. Crystallite distribution C_n at $T = 1.75(O)$, $1.8(X)$, $1.85(+)$, and $1.9(*)$. The distribution at $T = 1.75$ is likely to be less accurate than the others because of its proximity to the phase transition.

melting point is small. The clusters tend to be closer to the compact extreme. The low number of directional interactions for some of the large clusters at $T = 1.85$ is likely an artifact of the poor statistics for clusters of this size. The clusters at $T = 1.3$ long after the quench from $T = 25.0$ discussed below are more compact than those above the melting point, as would be expected if the state of the clusters in the supercooled medium reflected the degree of undercooling.

V. FREEZING DYNAMICS

We have simulated the freezing dynamics of two types of quenches with both R_I values: (1) an instantaneous quench with $\rho = 0.25$ from $T = 25.0$ (essentially infinity) to a fixed temperature below the melting point and (2) a slow cooling from above the melting point with $\rho = 0.125$ in which the temperature is lowered by 0.05 units every

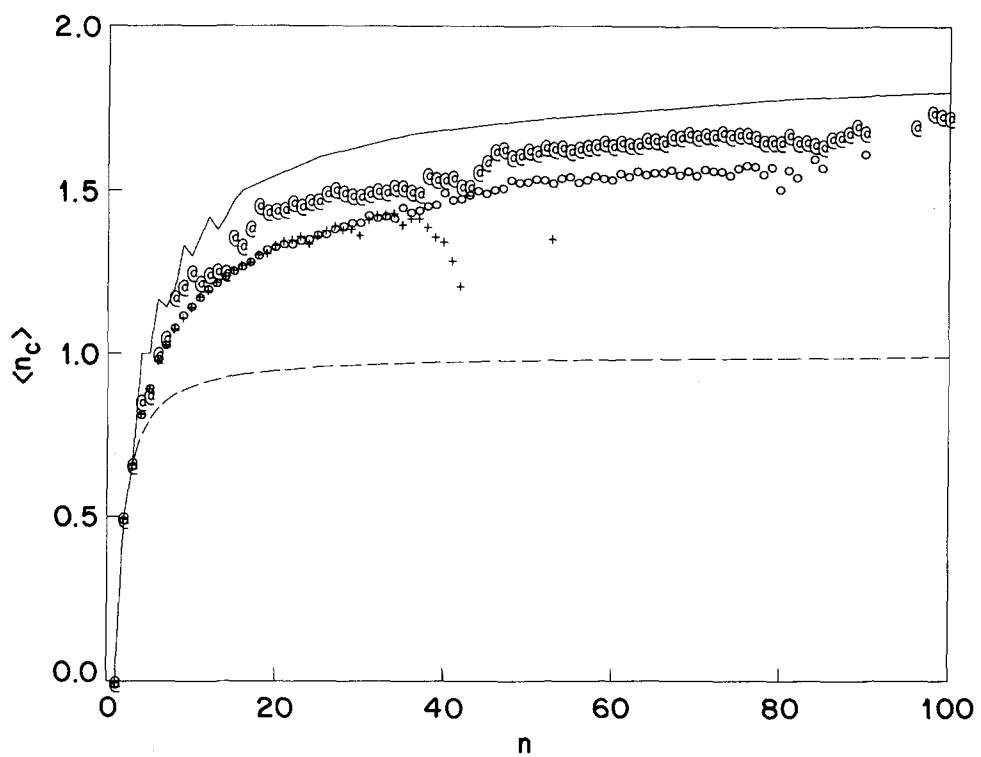

FIG. 7. Average number of directional interactions per molecule, $\langle n_C \rangle$, of crystals of size n at some of the same temperatures used in Fig. 6. The solid line is the energy of the most compact clusters possible and the dashed line is the energy of the most extended clusters possible (lines of molecules). The "@" correspond to averages over $20\,000\tau$ taken during an interval starting $104\,000\tau$ after a quench to $T = 1.3$ ($R_I = 1.0$).

125 000τ. In both cases, we generate the stochastic dynamics of the system using the Metropolis algorithm as described in Sec. III.

When $\rho = 0.25$ and $R_I = 1$, freezing proceeds by the rapid formation of small crystallites, followed by a very slow annealing process in which the crystallites flocculate. Instantaneous quenches to $T = 1.7$, 1.5, 1.3, 1.1, and 0.9 on a 40×40 lattice have been examined. Within the first 150τ, quenches to $T = 1.3$ produce the lowest (most negative) directional interaction energies.

We then repeated selected runs on an 80×80 lattice (1600 molecules at $\rho = 0.25$). At $T = 1.7$ the temperature is so close to the melting point that the system can experience occasional increases in the directional interaction energy, even long after the initial quench. At the end of this quench, three clusters each containing more than 300 molecules dominate the system. The kinetics are illustrated by the decrease in the directional interaction energy (Fig. 8) and the distribution of molecules which interact with 0, 1, 2, 3, and 4 neighboring molecules through the directional interaction (Fig. 9). For temperatures of $T = 1.1$ and lower, the decrease in the directional interaction energy becomes slower.

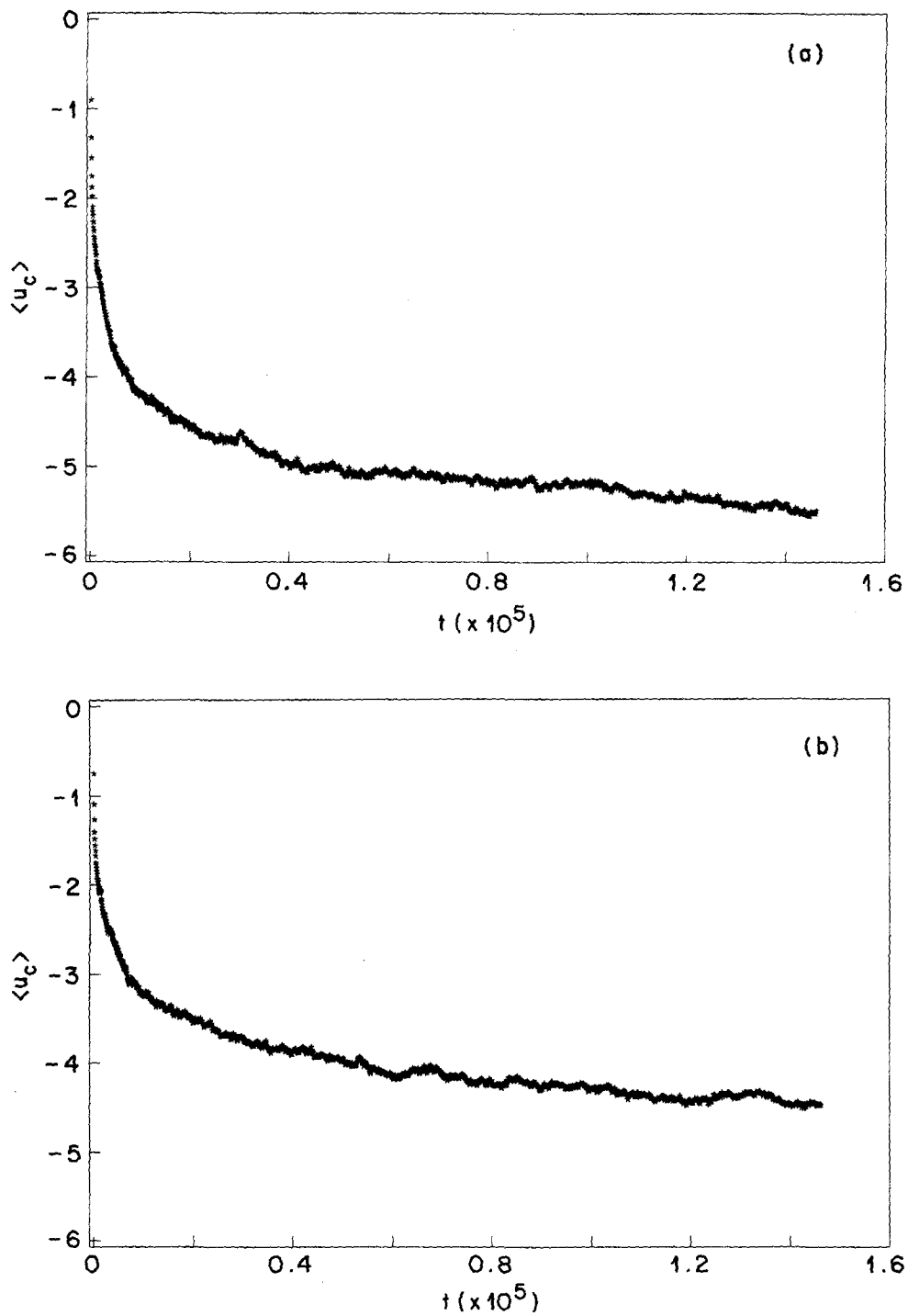

FIG. 8. Directional interaction energy decrease during quenches from $T = \infty$ to (a) $T = 1.3$ ($R_I = 1$), (b) $T = 1.3$ ($R_I = 0$), (c) $T = 1.65$ ($R_I = 1$), and (d) $T = 1.7$ ($R_I = 1$).

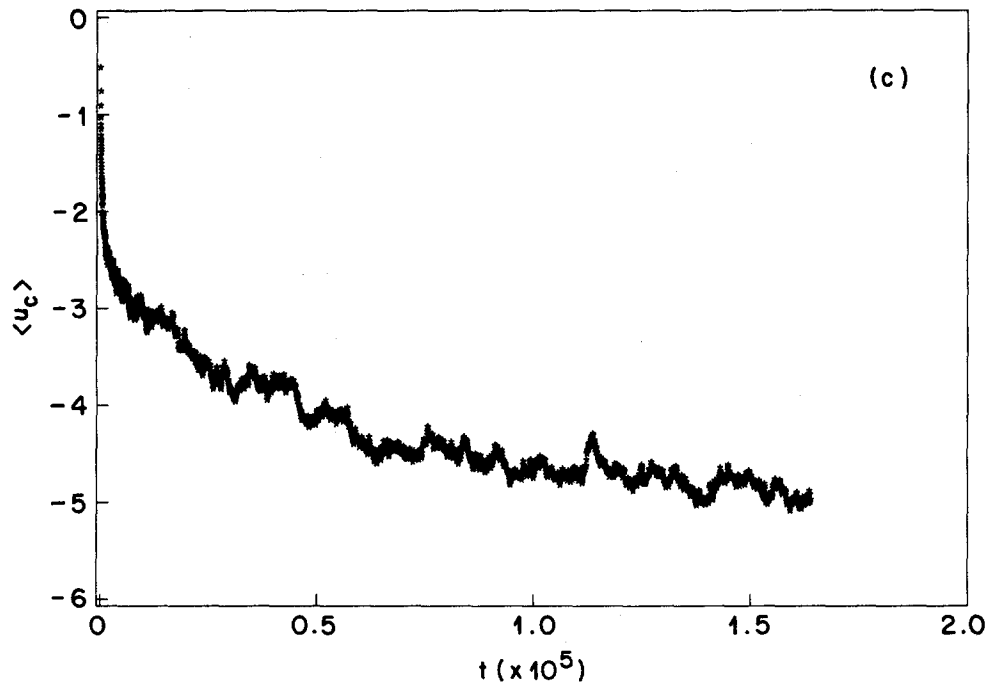

FIG. 8 (*continued*).

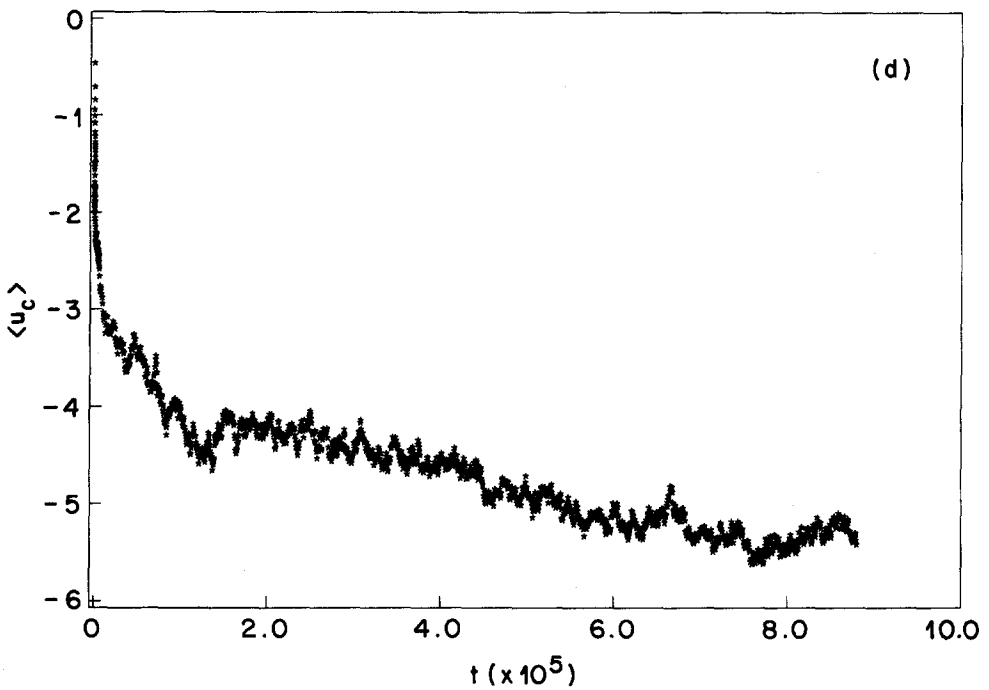

When the isomerization is allowed, in the early stage of the quench the number of molecules with 1 and 2 directional interactions increases almost instantaneously, while the fraction of molecules experiencing no such interactions drops from over 80% to less than 10% within the first 1500τ. At $T = 1.3$ the fraction of molecules with three directional interactions, which lie at the crystallite surfaces, or adjacent to rare defects in the bulk, reaches a maximum at about $20\,000\tau$. The rest of the simulation is characterized by a gradual increase in the number of molecules with four interactions, namely, those lying at the center of a crystallite. This occurs as crystallites flocculate and grain boundaries disappear.

For systems as large as 80×80, our simulations are too short to observe complete spontaneous optical resolution of the entire system, although there is little doubt that eventual-

ly this would occur. In 20×20 lattices, we have seen the liquid freeze into a single optically active crystal within one simulation.

When the inversion is forbidden, the chirality becomes a conserved order parameter. The freezing is much slower, because after the molecules initially bind to nearby neighbors with the same chiralities, the coarsening by cluster growth becomes diffusion limited. Since molecules at an interface of differing chiralities cannot interconvert, that interface is essentially pinned. The diffusion is too slow to allow significant coarsening to occur during these simulations. The influence of the inversion process on the crystal growth rate at $T = 1.3$ can be seen in the comparison between portions of configurations $150\,000\tau$ after the quench in systems with $R_I = 1$ [Fig. 10(a)] and with $R_I = 0$ [Fig. 10(b)]. Clearly the grains of the system with no isomerization are finer. The contrast between these two cases is also shown by the differences in the rate of change of the directional inter-

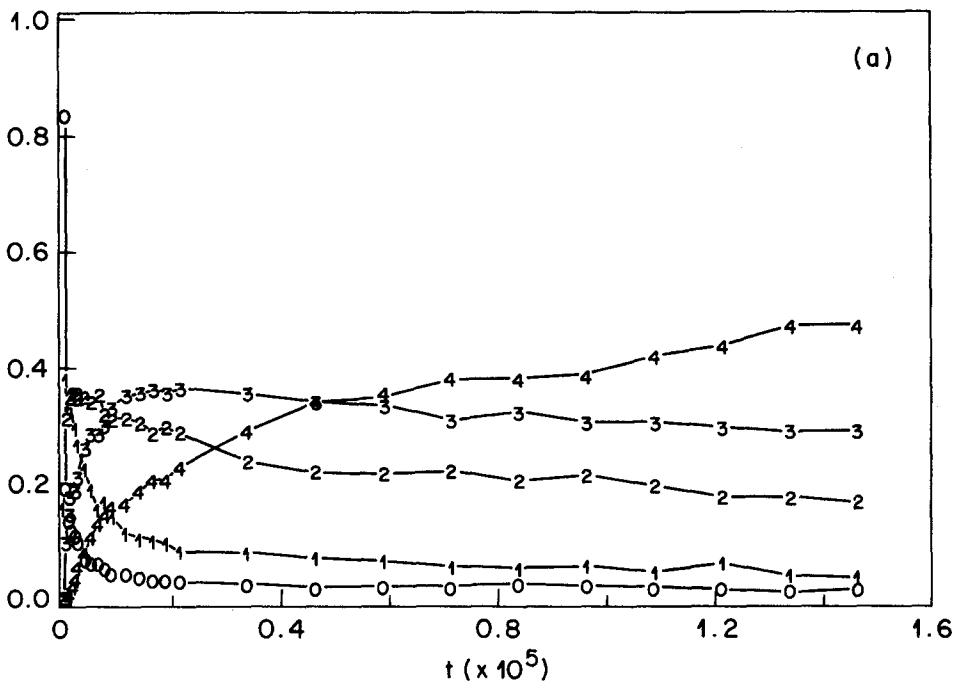

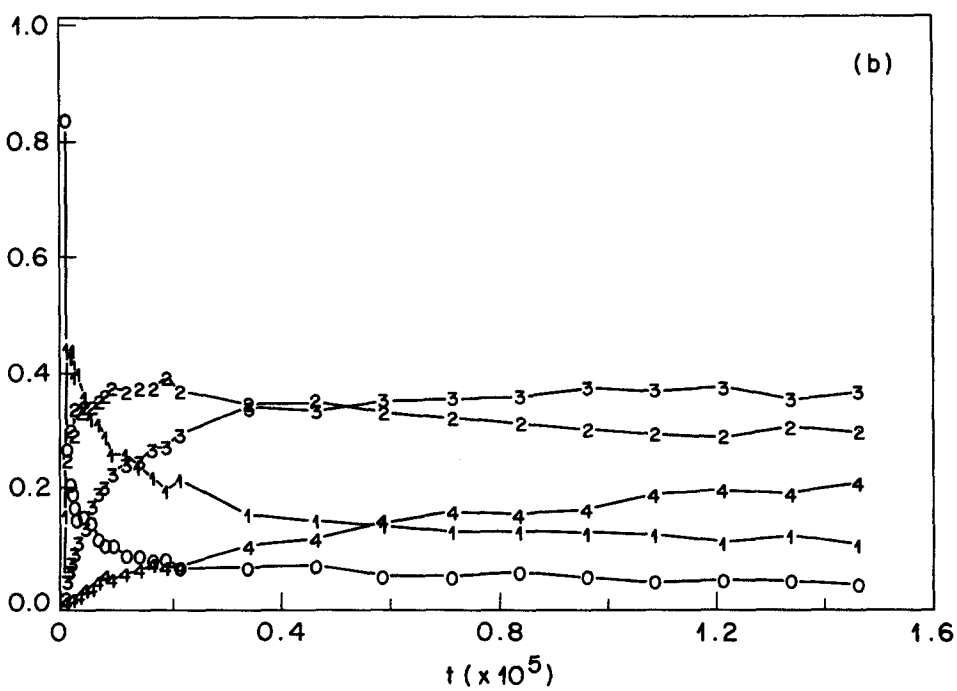

FIG. 9. Fraction of molecules with 0, 1, 2, 3, and 4 orientational interactions where the numbers are used as symbols in the graph. (a)–(d) correspond to the same simulations shown in the previous graphs.

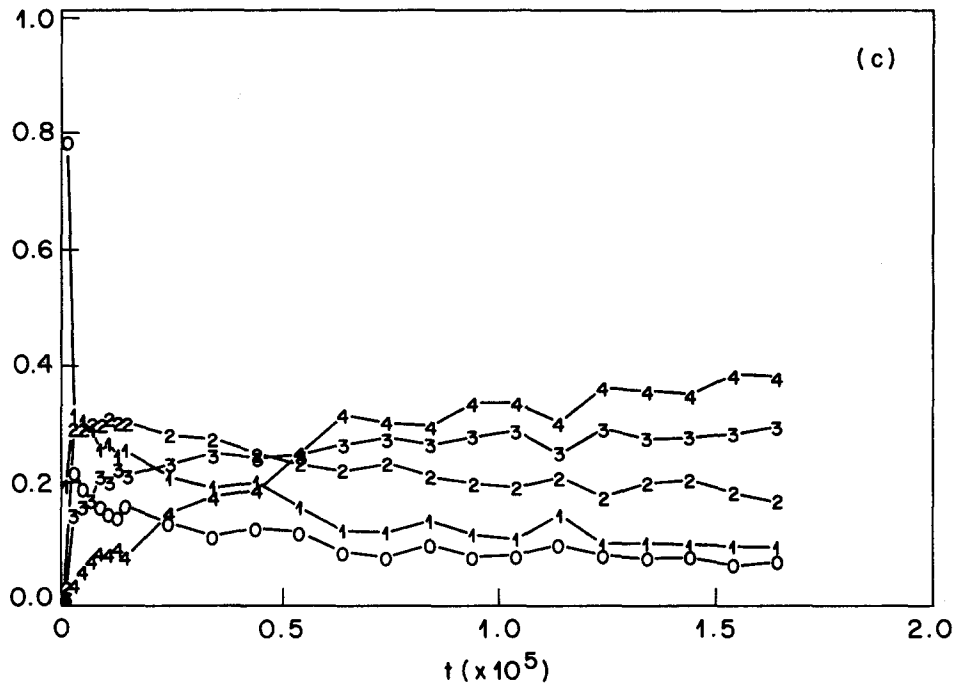

FIG. 9 (*continued*).

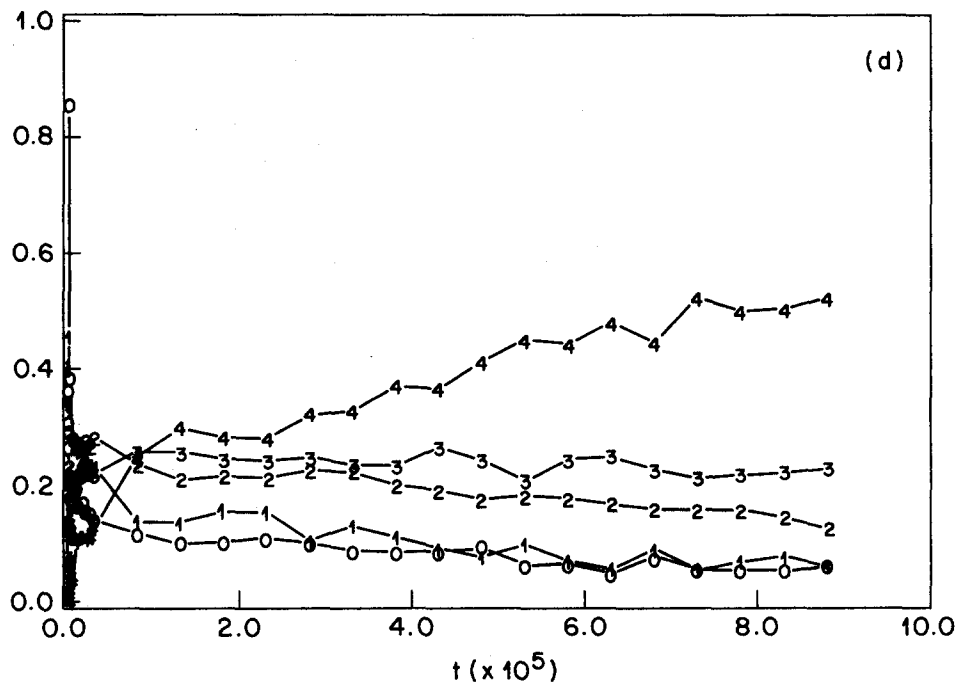

action energy per molecule [Figs. 8(a), 8(b), 9(a), and 9(b)].

The relatively small size of our systems makes a determination of the critical cluster size difficult. The number of crystallites consisting of between five and fifteen molecules is too small to find the parameters in Eq. (1) using a fit to the the cluster distribution in the simulation. We roughly estimate critical cluster sizes using the frequency of cluster growth and shrinkage as defined in Sec. III. Above the critical cluster size, the number of growths should exceed the number of shrinkages; and below the critical cluster size, the opposite should be observed. If the time between the two configurations used for the identification of child clusters (Sec. III), δt, is fairly short (i.e., 50–100τ at $T = 1.65$ or 1.70), for all cluster sizes more shrinkages are counted than growths (statistics averaged over 90 000τ). For this to be consistent with the overall growth of clusters, the average number of molecules added onto a cluster during a growth

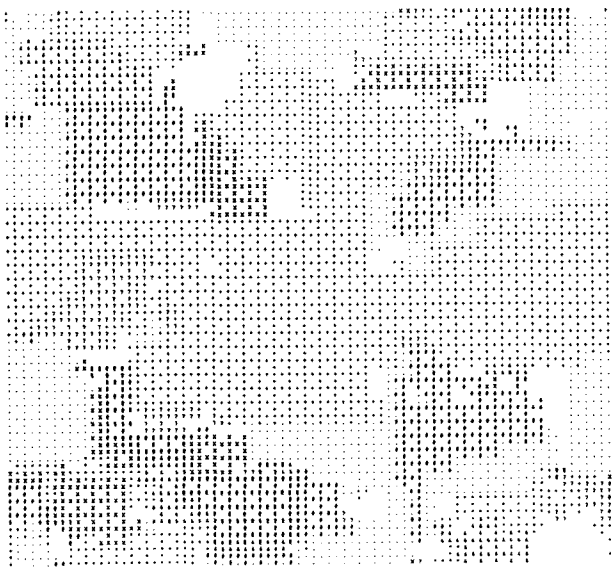

(a)

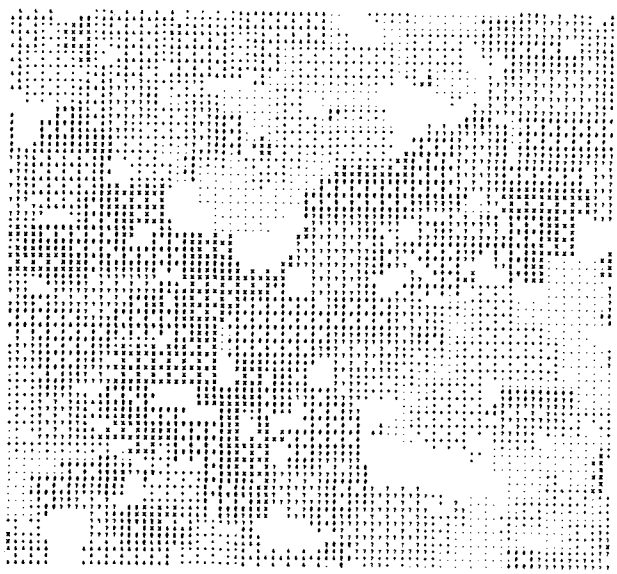

(b)

FIG. 10. Sample configurations at $150\,000\tau$ after the quench to $T = 1.3$ when (a) $R_I = 1$ and (b) $R_I = 0$. Each symbol represents a monomer of a different rotational-chiral state.

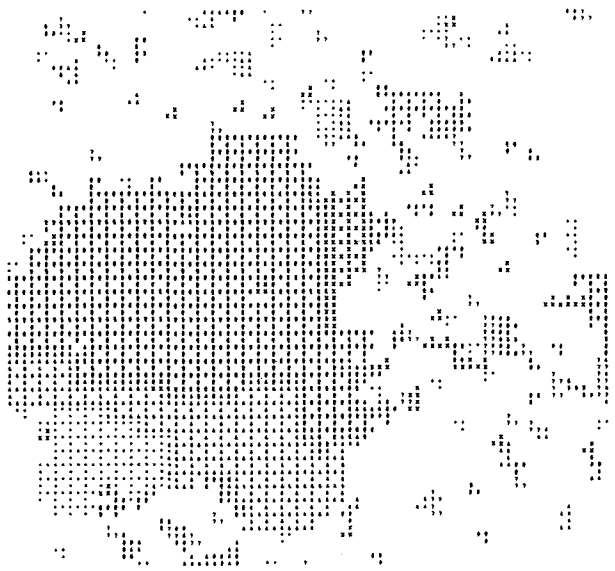

(a)

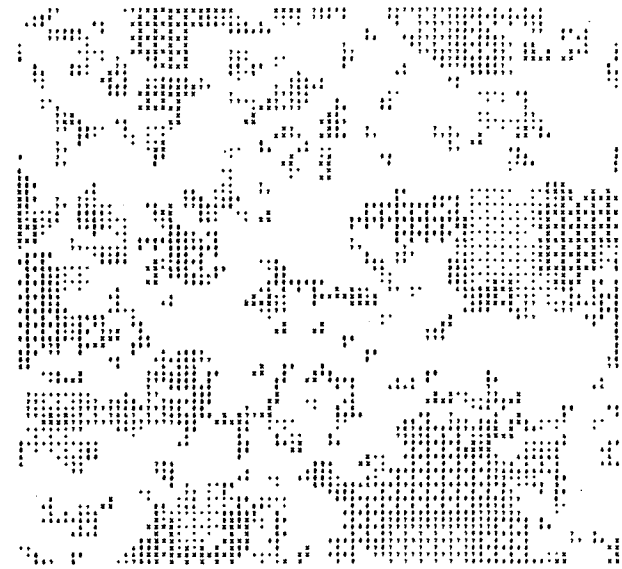

(b)

FIG. 11. Configurations at the end of the $T = 1.50$ segment of the slow undercooling when (a) $R_I = 1$ and (b) $R_I = 0$.

event must be greater than the number removed during a shrinkage. We use δt between 5000τ and $15\,000\tau$ to estimate the critical cluster sizes to be 5 at $T = 1.3$ ($\delta t = 12\,500\tau$), 15 at $T = 1.65$ ($\delta t = 10\,000\tau$), and 26 at $T = 1.70$ ($\delta t = 5000\tau$).

In the slow cooling with $\rho = 0.125$, the nucleation event is less ambiguous. At $T = 1.55$, a large single nucleus forms which eventually grows to become a crystal that accumulates additional material as the temperature is lowered. This is consistent with the overall classical picture of nucleation, although the scarcity of clusters larger than 10 atoms makes the estimation of a critical cluster size from this data difficult. It appears to be between 20 and 40 molecules. When $R_I = 0$, the nucleation process is inhibited and does not occur until the temperature reaches 1.5. Because diffusion is required for the growth of an optically active crystal, the rate of crystal growth is slowed enough so that several nuclei form "seed crystals" during the simulation. The differences between the undercoolings with the two values of R_I are shown in the configurations at the end of the $T = 1.5$ segment of the undercooling in Fig. 11.

An interesting feature of the chiral trimer model shown in the crystallization of the $\rho = 0.125$ system is the tendency of twinned crystals to form. Twinned crystals form easily

because the energy required to create the interdigitating grain boundary is fairly low, and once formed, it is pinned by its molecules' restricted motion. The grain boundary can be destroyed by diffusion of molecules on the surface or by the transport of molecules through the vapor phase. Because the grain boundary energy is independent of the chiralities of the molecules on either side, there is a probability 1/2 that a twinned crystal will include both isomers. If grown to a macroscopic size, each half of the twin would be optically active.

VI. DISCUSSION

The simulations reported in this work demonstrate that optical activity can be generated spontaneously from a racemic mixture through homogeneous nucleation and growth. This spontaneous optical resolution has been observed in several experimental systems.

Unlike previous lattice models used in nucleation studies, the present one incorporates an intramolecular conformational degree of freedom and an explicit exclusion interaction. This model cannot be reduced to a simple Potts model such as those used to study grain growth by Grest *et al.*[24]

Some previous isoenergetic molecular dynamics on quenched argon have observed a "time lag" between the quench and the release of latent heat associated with the catastrophic growth of a super-critical nucleus.[17] At none of the temperatures used in this work has such a phenomenon been observed.

Because "nuclei" of up to 20 molecules are fairly abundant in the liquid above the freezing point and clusters as large as 68 molecules have been observed in the liquid at $T = 1.8$, critical nuclei are present in relatively high concentrations in the liquid even before freezing except for extremely slight supercoolings. Furthermore, the nuclei grow most rapidly immediately after the quench but before the liquid coarsens substantially. All that is required to form a nucleus from the almost random distribution found immediately after a quench from a high temperature is a few rapid reorientations and inversions (when $R_I = 1$). After the initial nuclei form, the limiting step in the rate of heat release from the chiral trimer models is the motion of the grain boundaries. The shift of a grain boundary between even small clusters requires several concerted motions and frequently produces no change in the energy until one of the clusters is almost entirely consumed. Furthermore, this flocculation can only occur along half of the grain boundaries—those in which the molecules do not interdigitate.

The restrictions imposed by a lattice model play an important role in the rates of nucleus formation and grain boundary motion. In an off-lattice simulation, the small crystallites can be highly distorted so that a jump of a molecule from a small crystallite to a large one can be quite favorable. In our case, no such strain can occur in the smaller crystallites so that the concerted motions of several molecules is required before any decrease in potential energy is observed. Thus the limiting step in the growth of crystals in the chiral trimer model appears to be the motion of grain boundaries.

Previous theories predict that the grain size should increase as t^n where $n = 1/2$ for a nonconserved order parameter and $n = 1/3$ for a conserved one.[14,25,26] We can continuously vary the dynamics by lowering R_I to 0 so the chirality switches from a nonconserved to a conserved order parameter. Even when $R_I = 0$, the other order parameters, the orientation and the sublattice occupation, are nonconserved. Unfortunately our system size is too small and the simulations are too short to determine the variation of n with R_I for the chiral trimer model. To complete simulations long enough to determine whether the grain growth rate is similar to that observed in the Q-state, Potts models will require the modification of the simulation technique and dynamics, likely to an algorithm similar to that used by Bortz *et al.*[27] and Sahni *et al.*[28]

[1] B. S. Green, M. Lahav, and D. Rabinovich, Acc. Chem. Res. **12**, 191 (1979).
[2] J. Jacques, A. Collet, and S. H. Wilen, *Enantiomers, Racemates, and Resolutions* (Wiley, New York, 1981).
[3] L. W. Jelinski and E. F. Kiefer, J. Am. Chem. Soc. **98**, 281 (1976).
[4] E. Havinga, Biochim. Biophys. Acta **13**, 171 (1954).
[5] R. D. Gillard and F. L. Wimmer, J. Chem. Soc. Chem. Comm. 936 (1978).
[6] A. C. D. Newman and H. M. Powell, J. Chem. Soc. 3747 (1952).
[7] R. E. Pincock, R. R. Perkins, A. S. Ma, and K. R. Wilson, Science **174**, 1018 (1971).
[8] R. E. Pincock and K. R. Wilson, J. Chem. Ed. **50**, 455 (1973).
[9] K. R. Wilson and R. E. Pincock, J. Am. Chem. Soc. **97**, 1474 (1975).
[10] K. R. Wilson and R. E. Pincock, Can. J. Chem. **55**, 889 (1976).
[11] R. B. Kress, E. N. Duesler, M. C. Etter, I. C. Paul, and D. Y. Curtin, J. Am. Chem. Soc. **102**, 7709 (1980).
[12] R. Kuroda and S. F. Mason, J. Chem. Soc. Perkin II 167 (1981).
[13] A. C. Zettlemoyer, *Nucleation* (Marcel Dekker, New York, 1969).
[14] J. D. Gunton, in *Phase Transitions*, edited by C. Domb and J. L. Lebowitz (Academic, London, 1983), Vol. 8, p. 267.
[15] S. R. Stiffler, M. O. Thompson, and P. S. Peercy, Phys. Rev. Lett. **60**, 2519 (1988).
[16] W. Swope and H. C. Andersen (preprint).
[17] M. J. Mandell, J. P. McTague, and A. Rahman, J. Chem. Phys. **64**, 3699 (1976).
[18] R. D. Mountain and P. K. Basu, J. Chem. Phys. **73**, 7318 (1983).
[19] K. Binder, Adv. Colloid Interface Sci. **7**, 279 (1977).
[20] D. Stauffer, A. Coniglio, and D. W. Heermann, Phys. Rev. Lett. **49**, 1299 (1982).
[21] I. Edrei and M. Gitterman, J. Phys. A **19**, 3279 (1986).
[22] N. Metropolis, A. W. Rosenbluth, M. N. Rosenbluth, A. H. Teller, and E. Teller, J. Chem. Phys. **21**, 1087 (1953).
[23] F. Y. Wu, Rev. Mod. Phys. **54**, 235 (1982).
[24] G. S. Grest, M. P. Anderson, and D. J. Srolovitz, Phys. Rev. B **38**, 4752 (1988).
[25] S. M. Allen and J. W. Cahn, Acta Metall. **27**, 1085 (1979).
[26] I. M. Lifshitz and V. V. Slyozov, J. Phys. Chem. Solids **19**, 35 (1961).
[27] A. B. Bortz, M. H. Kalos, and J. L. Lebowitz, J. Comp. Phys. **17**, 10 (1975).
[28] P. S. Sahni, D. J. Srolovitz, G. S. Grest, M. P. Anderson, and S. A. Safran, Phys. Rev. B **28**, 2705 (1983).